catalysts

MDPI

Article

Oxy-Steam Reforming of Liquefied Natural Gas (LNG) on Mono- and Bimetallic (Ag, Pt, Pd or Ru)/Ni Catalysts

Pawel Mierczynski [1,*], Magdalena Mosinska [1], Waldemar Maniukiewicz [1], Krasimir Vasilev [2] and Malgorzata Iwona Szynkowska-Jozwik [1]

[1] Faculty of Chemistry, Institute of General and Ecological Chemistry, Lodz University of Technology, Zeromskiego 116, 90-924 Lodz, Poland; magdalena.mosinska@dokt.p.lodz.pl (M.M.); waldemar.maniukiewicz@p.lodz.pl (W.M.); malgorzata.szynkowska@p.lodz.pl (M.I.S.-J.)

[2] School of Engineering, University of South Australia, Mawson Lakes, Adelaide, SA 5095, Australia; krasimir.vasilev@unisa.edu.au

* Correspondence: pawel.mierczynski@p.lodz.pl; Tel.: +48-42-631-3125

Abstract: This work presents, for the first time, the comparative physicochemical and reactivity studies of a range of bimetallic Pt-Ni, Pd-Ni, Ru-Ni, and Ag-Ni catalysts in the oxy-steam reforming (OSR) of liquefied natural gas (LNG) reaction towards hydrogen generation. In order to achieve the intended purpose of this work, a binary oxide CeO_2·ZrO_2 (1:2) support was prepared via a co-precipitation method. The catalysts' physicochemical properties were studied using X-ray diffraction (XRD), BET, TPR-H_2, TPD-NH_3, SEM-EDS and XPS methods. The highest activity in the studied process was exhibited by the 1%Pt-5%Ni catalyst supported on CeO_2·ZrO_2 (1:2) system. The highest activity of this system is explained by the specific interactions occurring between the components of the active phase and between the components of the active phase and the carrier itself. The activity results showed that this catalytic system exhibited above 71% of the methane conversion at 600 °C and 60% yield of hydrogen formation. The results of this work demonstrate that the Pt-Ni and Ru-Ni catalytic systems hold promise to be applied in the production of hydrogen to power solid oxide fuel cells.

Keywords: noble metal; bimetallic catalyst; nickel catalyst; hydrogen production; oxy-steam reforming; LNG; hydrogen production

Citation: Mierczynski, P.; Mosinska, M.; Maniukiewicz, W.; Vasilev, K.; Szynkowska-Jozwik, M.I. Oxy-Steam Reforming of Liquefied Natural Gas (LNG) on Mono- and Bimetallic (Ag, Pt, Pd or Ru)/Ni Catalysts. *Catalysts* **2021**, *11*, 1401. https://doi.org/10.3390/catal11111401

Academic Editors: Patrick Da Costa and Leonarda Francesca Liotta

Received: 24 September 2021
Accepted: 15 November 2021
Published: 19 November 2021

1. Introduction

The deteriorating state of the environment and constantly rising energy prices have risen the community and political awareness about the urgent need for alternative energy sources which could make society and industry independent from burning fossil materials [1]. One possible solution with high potential is hydrogen. Energy produced from hydrogen is potentially one of the cleanest and inexhaustible sources. Unlike fossil fuels, only water and electricity are produced in a fuel cell [2,3]. Hydrogen can be produced from fossil fuels (natural gas, petroleum and coal) and by water electrolysis. Hydrogen can also be obtained by reforming of hydrocarbons or alcohols [4–7]. The technology based on the steam reforming of methane has proven to be suitable for industrial hydrogen production. Liquefied natural gas (LNG) also has many advantages. The LNG consists mainly of methane (88–99%) and other light hydrocarbons and nitrogen [8–11]. Liquefying natural gas results in a clean, odourless, and colourless gas mixture with non-toxic and non-corrosive properties [12]. Additionally, the constantly expanding pipe infrastructure provides favourable conditions for the future LNG distribution and effective use in hydrogen production [13,14]. Nickel catalysts are widely used in the reforming of liquefied natural gas (LNG) [8,12–18]. The use of nickel catalysts requires a high reaction temperature and an excess of steam to prevent the formation of carbon deposits during the reforming

process [19]. ZrO_2 supports were reported to increase the steam adsorption on the catalyst surface, which caused increased efficiency of the hydrocarbon gasification process, leading to enhanced hydrogen production and decreased coke deposition on the catalyst surface [17,20]. Therefore, nickel catalysts supported on ZrO_2 or supports containing this oxide exhibit better catalytic performance in steam reforming reactions [8]. The addition of CeO_2 to Ni catalysts improves their stability, provides mobile oxygen and prevents the formation of carbon deposits, which improves the activity of the catalyst [21–23]. It is well documented and confirmed in our previous works [4–7,24,25] that the addition of precious metals (Rh, Pd, Ru, Ag and Ir) to monometallic nickel or copper catalysts has a significant impact on their activity and selectivity in the studied reactions. Bimetallic catalysts often exhibited higher activity compared to the monometallic catalysts in the steam and oxy-steam reforming of methanol or water gas shift (WGS) reactions. This is often associated with the formation of an alloy between Ni/Cu and the noble metal and/or the spillover effect which leads to an increase of the catalyst activity and hydrogen formation efficiency. We proved in those works that addition of precious metals to nickel or copper based catalysts had a great impact on their acidity, reducibility and dispersion of the active phase on the catalyst surface which are the main factors determining their reactivity in the tested reactions.

In this paper, we evaluated the catalytic activity of Ni and bimetallic (Ag, Pt, Pd or Ru)/Ni catalysts. The main goal of the presented work was to determine the effect of noble metal (Ag, Pt, Pd or Ru) addition on the physicochemical and reactivity properties of $Ni/CeO_2{\cdot}ZrO_2$ (1:2) catalyst in the oxy-steam reforming of liquefied natural gas (OSR-LNG). To achieve the main goal of this paper, the support was prepared by a co-precipitation method, whereas, the mono- and bimetallic catalysts were prepared by an impregnation method. The physicochemical properties of the investigated catalytic systems were determined by the following techniques: TPR-H_2, BET, TPD-NH_3, XRD, SEM-EDS and XPS. Activity tests were performed in the oxy-steam reforming of liquefied natural gas (OSR-LNG) process using a fixed-bed microreactor. In addition, the catalytic activity measurements were correlated with the physicochemical properties of the studied catalytic materials.

2. Results and Discussion

2.1. Activity Tests

The catalytic activity measurements were performed in an oxy-steam reforming of liquefied natural gas reaction (OSR-LNG). Activity tests were carried out in a quartz microreactor in the temperature range 400–900 °C. The activity results are expressed as hydrocarbons (methane, ethane, propane and butane) conversions, selectivity to CO and CO_2 production, and hydrogen yield (see Tables 1 and 2). The results obtained for the monometallic 5% $Ni/CeO_2{\cdot}ZrO_2$ (1:2) catalyst showed that this catalytic system exhibited high methane conversion value (100%) at 900 °C. In the case of this system, we also already observed the total conversion (100%) of higher hydrocarbons (ethane, propane and butane) at 600 °C. Introduction of Pt and Ru metals into the monometallic Ni catalyst resulted in an increase of the methane conversion to 100% at 800 °C. The 1% Pt-5% $Ni/CeO_2{\cdot}ZrO_2$ (1:2) catalyst showed 100% conversion of ethane, propane, and butane even at 500 °C. For this system, methane conversion was 26% at 500 °C. This was the highest value of all investigated catalytic systems in the oxy-steam reforming of LNG process. At 500 °C, only in the case of the 1% Pt-5% $Ni/CeO_2{\cdot}ZrO_2$ (1:2) catalyst the formation of hydrogen was confirmed which exhibited the hydrogen yield 44% (see Table 2). These results confirmed that the bimetallic 1% Pt-5% $Ni/CeO_2{\cdot}ZrO_2$ (1:2) catalyst was the most active catalyst at 400 and 500 °C, respectively. On the other hand, the nickel catalysts promoted by palladium or silver exhibited lower hydrocarbon conversion in the studied temperature range compared to the monometallic Ni catalyst. The 1% Ag-5% $Ni/CeO_2{\cdot}ZrO_2$ (1:2) catalytic system showed the lowest hydrocarbon conversion in the OSR-LNG reaction (64% of methane, 97% for ethane, 100% for propane and 100% for butane) at 900 °C.

Table 1. Activity of mono- and bimetallic catalysts supported on $CeO_2 \cdot ZrO_2$ (1:2) tested in OSR-LNG.

Catalysts	Temperature (°C)	Methane Conversion (%)	Ethane Conversion (%)	Propane Conversion (%)	Butane Conversion (%)
5% $Ni/CeO_2 \cdot ZrO_2$ (1:2)	400	3	7	19	64
	500	11	55	89	100
	600	79	100	100	100
	700	97	100	100	100
	800	90	100	100	100
	900	100	100	100	100
1%Ru-5%$Ni/CeO_2 \cdot ZrO_2$ (1:2)	400	2	49	98	100
	500	6	54	91	100
	600	76	100	100	100
	700	98	100	100	100
	800	100	100	100	100
	900	100	100	100	100
1%Pd-5% $Ni/CeO_2 \cdot ZrO_2$ (1:2)	400	6	10	17	100
	500	4	13	26	100
	600	38	99	100	100
	700	62	100	100	100
	800	89	100	100	100
	900	97	100	100	100
1%Pt-5%$Ni/CeO_2 \cdot ZrO_2$ (1:2)	400	8	70	96	100
	500	26	100	100	100
	600	71	100	100	100
	700	96	100	100	100
	800	100	100	100	100
	900	100	100	100	100
1%Ag-5% $Ni/CeO_2 \cdot ZrO_2$ (1:2)	400	5	11	23	100
	500	10	39	76	100
	600	13	37	63	100
	700	18	48	73	100
	800	29	72	91	100
	900	64	97	100	100

Further analysis of the selectivity of the investigated catalysts towards CO and CO_2 formation and hydrogen yield showed that for the Ni-supported catalyst we can observe all main products (H_2, CO_2 and CO) in the outlet gases above 600 °C. The hydrogen yield for this catalyst reached about 60% in the temperature range 600–900 °C. Furthermore, the monometallic nickel catalyst exhibited the highest selectivity to CO_2 and the lowest selectivity to CO at 600 °C. In contrast, the catalytic activity test carried out on the bimetallic catalysts showed that the highest catalytic activity was observed over the 1% Pt-5% $Ni/CeO_2 \cdot ZrO_2$ (1:2) catalyst, for which we observed H_2 and CO_2 formation at 500 °C. This catalyst reached high values of H_2 yield (60%) and selectivity toward CO_2 production (48%) and low selectivity to CO (52%) at 600 °C compared to the other studied systems. The 1% Ru-5% $Ni/CeO_2 \cdot ZrO_2$ (1:2) catalyst exhibited also similar catalytic activity at 600 °C as the 1% Pt-5% $Ni/CeO_2 \cdot ZrO_2$ (1:2) catalytic system. The lowest activity in the OSR-LNG process compared to all other investigated catalytic systems corresponded to the 1% Ag-5% $Ni/CeO_2 \cdot ZrO_2$ (1:2) catalyst. It should be noted that for 1% Ag-5% $Ni/CeO_2 \cdot ZrO_2$ (1:2) catalyst, hydrogen was formed above 600 °C. The catalytic tests results for bimetallic catalysts also showed that an increased reaction temperature caused increasing selectivity toward CO production. Moreover, comparing the activities of 5% $Ni/CeO_2 \cdot ZrO_2$ (1:2) and 1% Pt-5% $Ni/CeO_2 \cdot ZrO_2$ (1:2) catalysts at the temperature of 600 °C, we observed that the OSR-LNG reaction carried out on a bimetallic system leads to a slightly higher hydrogen production efficiency and CO_2 formation selectivity, and lower CO selectivity.

Table 2. Activity of mono- and bimetallic catalysts supported on $CeO_2 \cdot ZrO_2$ (1:2) system tested in OSR-LNG process.

Catalysts	Temperature (°C)	CO Selectivity (%)	CO_2 Selectivity (%)	H_2 Yield (%)
5% Ni/$CeO_2 \cdot ZrO_2$ (1:2)	400	0	100	0
	500	0	100	0
	600	66	34	59
	700	82	18	60
	800	78	22	61
	900	86	14	58
1%Ru-5%Ni/$CeO_2 \cdot ZrO_2$ (1:2)	400	0	100	0
	500	0	100	0
	600	50	50	60
	700	79	21	50
	800	87	13	57
	900	87	13	48
1%Pd-5% Ni/$CeO_2 \cdot ZrO_2$ (1:2)	400	0	100	0
	500	0	100	0
	600	0	100	35
	700	29	71	47
	800	62	38	59
	900	71	29	57
1%Pt-5%Ni/$CeO_2 \cdot ZrO_2$ (1:2)	400	0	100	0
	500	0	100	44
	600	52	48	60
	700	72	28	55
	800	84	16	52
	900	85	15	54
1%Ag-5% Ni/$CeO_2 \cdot ZrO_2$ (1:2)	400	0	100	0
	500	0	100	0
	600	0	100	0
	700	3	97	57
	800	14	86	45
	900	73	27	56

It should be also noticed that 1% Ru-5% Ni/$CeO_2 \cdot ZrO_2$ (1:2) catalysts exhibited very similar activity to the 1% Pt-5% Ni/$CeO_2 \cdot ZrO_2$ (1:2) system in the studied process. It demonstrated 76% of methane conversion and total conversions of ethane, propane and butane at 600 °C. In addition, this system exhibited 60% of hydrogen yield, 52 and 48% selectivity to CO and CO_2, respectively. These results confirmed the possibility of using bimetallic 1% Pt-5% Ni/$CeO_2 \cdot ZrO_2$ (1:2) catalyst in oxy-steam reforming of LNG process for hydrogen generation to power fuel cells in a low temperature range.

2.2. Temperature Programmed Reduction (TPR-H_2) Measurements

The reduction behaviours of the investigated catalytic systems were examined using temperature-programmed reduction techniques. TPR-H_2 profiles recorded for support, mono- and bimetallic supported catalysts are given in Figure 1 and Table 3. The temperature programmed reduction curve obtained for the $CeO_2 \cdot ZrO_2$ (1:2) support presents two unresolved reduction effects in the temperature range 250–650 °C. These reduction stages with maxima of hydrogen consumption peaks at 350 and 540 °C are associated with a surface reduction of CeO_2 species and with a reduction of bulk CeO_2 to Ce_2O_3 [7,26,27]. The significant intensity of these peaks suggests that oxygen located within the subsurface or in the bulk of the binary support migrates to the surface along with a surface oxygen consumption which suggests high lattice oxygen mobility [28]. TPR-H_2 profile recorded for the 5%Ni/$CeO_2 \cdot ZrO_2$ (1:2) catalyst showed four unresolved reduction effects in the temperature range of 150–900 °C. The first effect of maximum hydrogen consumption at 230 °C is assigned to the reduction of unbounded NiO species. Second, the reduction effect

with the maximum hydrogen consumption at 340 °C is associated with the reduction of nickel oxide strongly interacting with the support. The third reduction stage above 435 °C is assigned to the reduction of CeO_2 surface species [29]. The last reduction peak encountered on the TPR profile at 750 °C is assigned to the reduction of the bulk CeO_2 system. The TPR-H_2 curve recorded for 1%Ag-5%Ni/CeO_2·ZrO_2 (1:2) catalyst showed six reduction effects in the temperature range of 50–900 °C. The first three unresolved reduction stages were located at 75 °C, 140 °C and 180 °C. The first effect is associated with the reduction of Ag_2O species. The second reduction peak is probably connected with the reduction of NiO interacting with metallic silver, which facilitates the reduction of NiO via a spillover effect. The third partially resolved reduction stage is assigned to the reduction of NiO species weakly interacting with the support. The reduction effects observed at 324 and 440 °C were attributed to the reduction of NiO interacting with the support and to a surface reduction of CeO_2 species, respectively. The last reduction effect in the high temperature range is connected with the reduction of bulk CeO_2 species. The reduction profile recorded for 1%Ru-5%Ni/CeO_2·ZrO_2 (1:2) catalyst showed four reduction effects. The first two stages are assigned to the reduction of $Ru^{4+} \rightarrow Ru^{2+} \rightarrow Ru^0$. In addition, the high intensity of the second reduction step visible on the TPR curve recorded for Ru-Ni catalysts suggest that this effect is also connected with the reduction of NiO species interacted with the metallic Ru via a spillover effect. The third TPR effect with the maximum of the hydrogen consumption rate located at 290 °C is connected with NiO species interacting with the support. The next reduction peak with the maximum of hydrogen consumption located at 435 °C is related to the reduction of CeO_2 surface species reduction. The TPR profile recorded for 1%Pt-5%Ni/CeO_2·ZrO_2 (1:2) catalyst is given in Figure 1. The TPR-H_2 profile recorded for this system showed three reduction stages. Two unresolved reduction effects in the temperature range 170–400 °C are assigned to the reduction of weakly and strongly interacted with the support NiO species, respectively. In addition, the absence of independent reduction peak for platinum oxide may also confirm that PtO is also reduced in the temperature range 170–270 °C [30]. The last reduction peak situated at high temperature (470 °C) is attributed to the reduction of CeO_2 surface species. The last reduction curve presents the TPR-H_2 profile recorded for the 1%Pd-5%Ni/CeO_2·ZrO_2 (1:2) catalyst. TPR-H_2 profile of 1%Pd-5%Ni/CeO_2·ZrO_2 (1:2) catalyst showed five reduction effects. The first reduction stage with the maximum of H_2 consumption peak located at 85 °C is associated with the reduction of PdO to Pd [31,32]. The next unresolved reduction peak centred at 120 °C is assigned to the reduction of NiO species interacted with metallic Pd via a spillover effect. The reduction effects in the temperature range of 220–400 °C are attributed to the reduction of NiO species differently interacting with the support [5,7]. The last reduction stage positioned at 450 °C is connected with the reduction of surface CeO_2 species reduction.

To further confirm the promoting effect of noble metal on the reducibility of the nickel catalysts supported on the CeO_2·ZrO_2 (1:2) system, deconvolution of the observed reduction peaks recorded for both mono- and bimetallic catalysts was performed and the results presented in Table 3. The contribution of each peak to the total area of TPR peaks attributed to the reduction of various forms of nickel oxide and Ce containing species and their maxima are presented. The results presented in Table 3 confirmed that the addition of noble metals decreases the temperature of each peak attributable to the reduction of NiO species. The presence of the reduction peaks assigned to NiO species located at a lower temperature in the case of the bimetallic catalysts compared to monometallic Ni catalysts confirmed the occurrence of specific interaction between noble metals and nickel oxide. The shift of the reduction profiles attributed to the reduction of NiO species towards the lower temperature range proves that the addition of noble metals (Ag, Pd, Pt and Ru) facilitates the reduction of nickel oxide species. The occurrence of specific interactions in the case of bimetallic catalysts has a strong influence on the reactivity results. These reduction behaviours may also confirm the alloying process between the metal components of the active phase in the case of bimetallic catalysts [10].

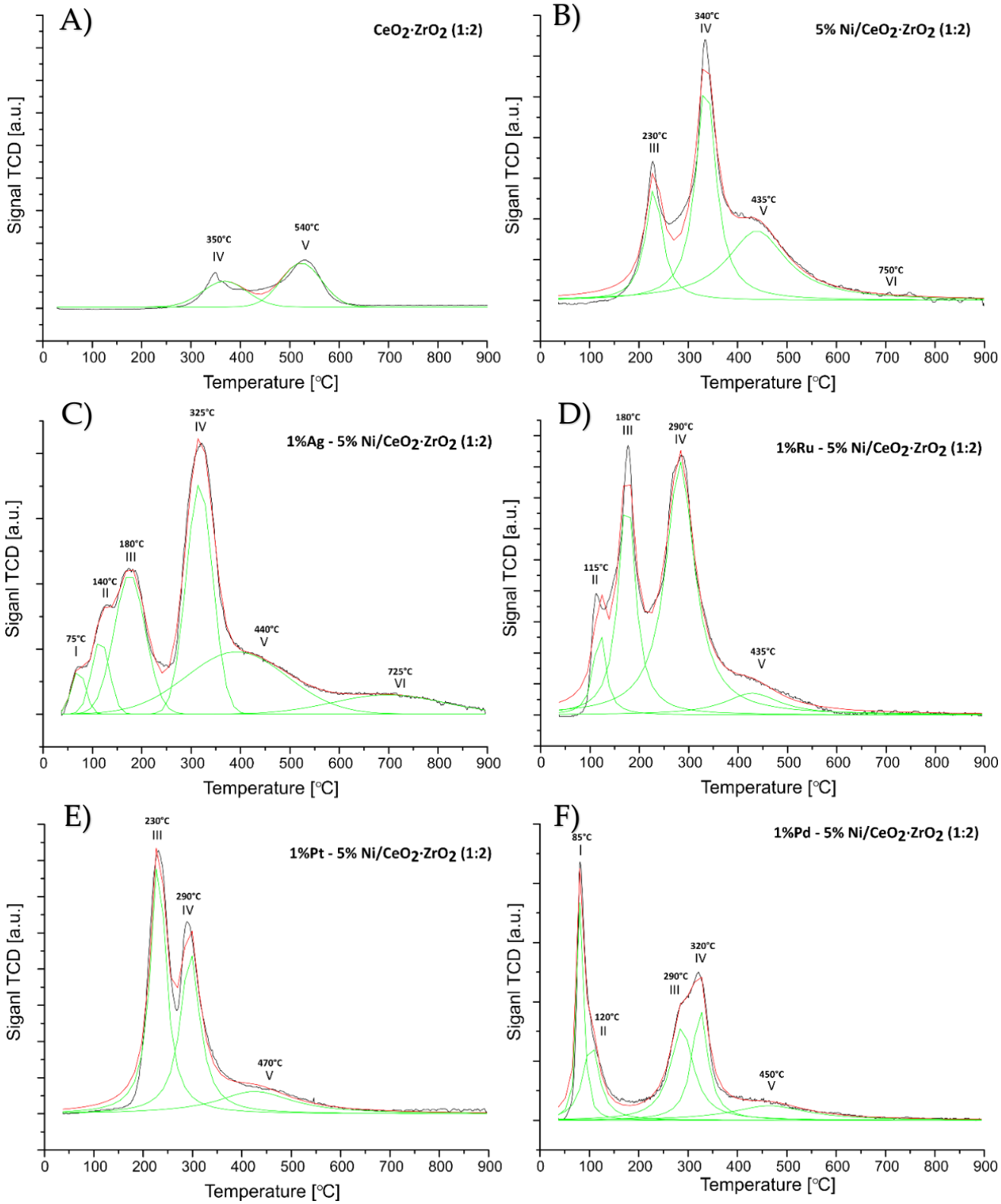

Figure 1. TPR-H_2 profiles for (**A**) support $CeO_2{\cdot}ZrO_2$ (1:2), monometallic (**B**) 5%Ni/$CeO_2{\cdot}ZrO_2$ (1:2) and bimetallic catalysts (**C**) 1%Ag-5%Ni/$CeO_2{\cdot}ZrO_2$ (1:2) (**D**) 1%Ru-5%Ni/$CeO_2{\cdot}ZrO_2$ (1:2) (**E**) 1%Pt-5%Ni/$CeO_2{\cdot}ZrO_2$ (1:2) (**F**) 1%Pd-5%Ni/$CeO_2{\cdot}ZrO_2$ (1:2) calcined in an air atmosphere at 400 °C for 4 h.

Table 3. Reduction data for the monometallic Ni and bimetallic 1% (Ag, Ru, Pt, Pd)-5% Ni catalysts after calcination in an air atmosphere at 400 °C for 4h.

Catalysts	Peak Contribution to the Overall TPR Peak Area (%)					
	I-Peak	II-Peak	III-Peak	IV-Peak	V-Peak	VI-Peak
CeO_2·ZrO_2 (1:2)	-	-	-	39 (350 °C)	61 (540 °C)	-
5%Ni/CeO_2·ZrO_2 (1:2)	-	-	18 (230 °C)	42 (340 °C)	35 (435 °C)	5 (750 °C)
1%Ag-5%Ni/CeO_2·ZrO_2 (1:2)	3 (75 °C)	6 (140 °C)	21 (180 °C)	29 (325 °C)	30 (440 °C)	11 (725 °C)
1%Ru-5%Ni/CeO_2·ZrO_2 (1:2)	13 (115 °C)	25 (180 °C)		52 (290 °C)	10 (435 °C)	-
1%Pt-5%Ni/CeO_2·ZrO_2 (1:2)	-	-	45 (230 °C)	36 (290 °C)	19 (470 °C)	-
1%Pd-5%Ni/CeO_2·ZrO_2 (1:2)	18 (85 °C)	16 (120 °C)	28 (290 °C)	23 (320 °C)	15 (450 °C)	-

2.3. Temperature Programmed Desorption (TPD-NH_3) Analysis

The temperature-programmed desorption of ammonia measurement was used to determine the acidity of the investigated catalytic materials. The TPD-NH_3 results are shown in Table 4 and express the amount of NH_3 adsorbed to the surface during TPD analysis, and were calculated based on the area under the ammonia desorption peaks. The TPD measurements performed for CeO_2·ZrO_2 (1:2) support showed the highest total acidity and the highest amount of strong acid sites presented on the surface, which was equal to 0.93 mmol/g and 0.36 mmol/g, respectively. Introduction of a nickel oxide phase on the support surface caused the decrease in the acidity of the catalyst surface. The decrease in acidity in the case of mono- and bimetallic catalysts is connected with masking of the acidic centers by active phase components [10,33]. Before each acidity measurement, Ni and bimetallic catalysts were reduced in pure hydrogen at 500 °C for 1 h. The TPD desorption measurements gave evidence that the acidity values for all systems could be expressed by the following relationship: 1% Pt-5% Ni/CeO_2·ZrO_2 (1:2) < 1% Ag-5% Ni/CeO_2·ZrO_2 (1:2) < 1% Pd-5% Ni/CeO_2·ZrO_2 (1:2) < 5% Ni/CeO_2·ZrO_2 (1:2) < 1% Ru-5% Ni/CeO_2·ZrO_2 (1:2). Analyses of the TPD curves of the bimetallic catalysts showed the dominance of the weak centers present on the surface of the investigated catalysts. In the case of all investigated catalytic materials, the obtained results confirmed the occurrence of three types of acid centers (weak, medium, and strong), except for the 1% Pt-5% Ni/CeO_2·ZrO_2 (1:2) and 1% Ag-5% Ni/CeO_2·ZrO_2 catalysts for which the strong acid centers were not detected on their surface.

Table 4. The surface acidity of the studied catalytic materials expressed as the amount of NH_3 adsorbed on the surface calculated from the results recorded during TPD-NH_3 measurements for the support, monometallic Ni and bimetallic catalysts.

Catalytic Systems	Total Acidity (mmol/g)	Weak Centers (mmol/g)	Medium Centers (mmol/g)	Strong Centers (mmol/g)
	180–600 °C	180–300 °C	300–450 °C	450–600 °C
CeO_2·ZrO_2 (1:2)	0.93	0.26	0.31	0.36
5%Ni/CeO_2·ZrO_2 (1:2)	0.51	0.20	0.21	0.09
1%Ru-5%Ni/CeO_2·ZrO_2 (1:2)	0.52	0.32	0.18	0.01
1%Pd-5%Ni/CeO_2·ZrO_2 (1:2)	0.42	0.22	0.19	0.02
1%Pt-5%Ni/CeO_2·ZrO_2 (1:2)	0.24	0.19	0.03	-
1%Ag-5%Ni/CeO_2·ZrO_2 (1:2)	0.36	0.32	0.04	-

2.4. X-ray Diffraction (XRD) Studies

The phase composition studies of the investigated catalytic systems were performed using X-ray diffraction techniques. XRD patterns are given in Figure 2. The XRD measurement recorded for CeO_2·ZrO_2 (1:2) support itself showed the present of CeO_2 and ZrO_2 phases. Moreover, the obtained results showed that ZrO_2 phase occur in two crystallographic structures: monoclinic (ZrO_2-M) and tetragonal (ZrO_2-T), respectively. In the case of monometallic nickel catalyst supported on CeO_2·ZrO_2 (1:2) system, the analysis of the XRD measurement confirmed the presence of NiO, CeO_2, ZrO_2-M and ZrO_2-T phases in

the XRD pattern. The addition of small amounts of noble metals into the nickel catalyst did not cause any changes in the phase composition of bimetallic catalytic systems. The lack of diffraction peaks assigned to the noble metal, oxides, or metallic phases are related with the limitation of the XRD method which do not detect the crystals below 5 nm in size [24]. That is why for better understanding the interaction of noble metals with Ni, the catalytic systems with higher content of noble metals were prepared and tested using XRD "in situ" measurements. Figures 3–6 show the XRD patterns collected for the bimetallic 5% (Ag, Pt, Pd, Ru)-5%Ni/CeO_2·ZrO_2 (1:2) catalysts during the reduction process performed in a mixture of 5% H_2-95% Ar in a temperature range 50–850 °C. The XRD "in situ" studies during the reduction of the bimetallic catalysts were done for the system with the higher noble metals (5% wt. of metal) content in the bimetallic catalysts to observe the interaction between active phase components.

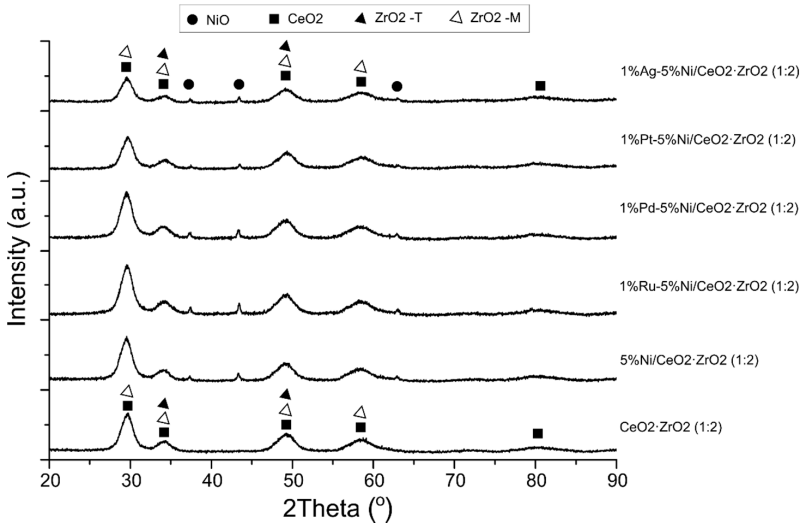

Figure 2. XRD patterns of the investigated support, mono- and bimetallic catalysts calcined in an air atmosphere at 400 °C for 4 h.

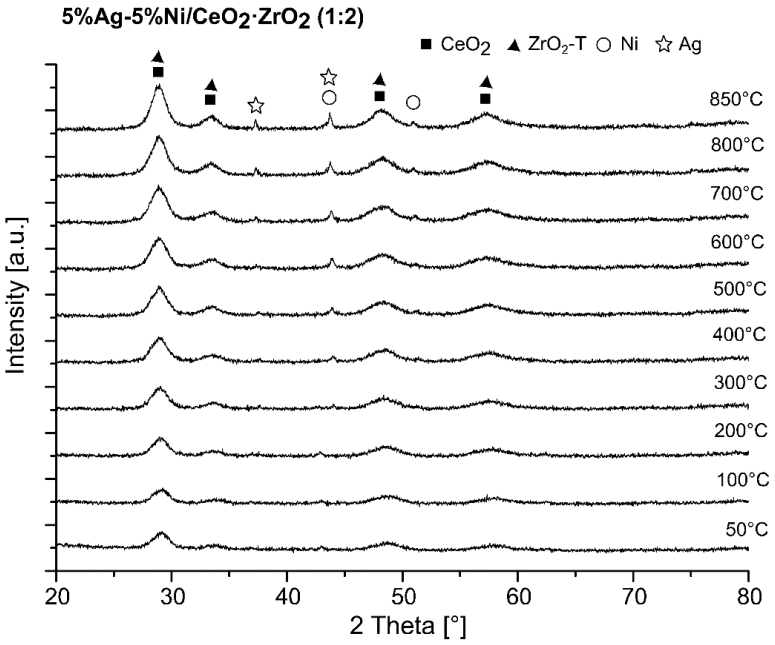

Figure 3. The X-ray diffraction measurements recorded for 5%Ag-5%Ni/CeO_2·ZrO_2 (1:2) catalyst performed the in-situ reduction process.

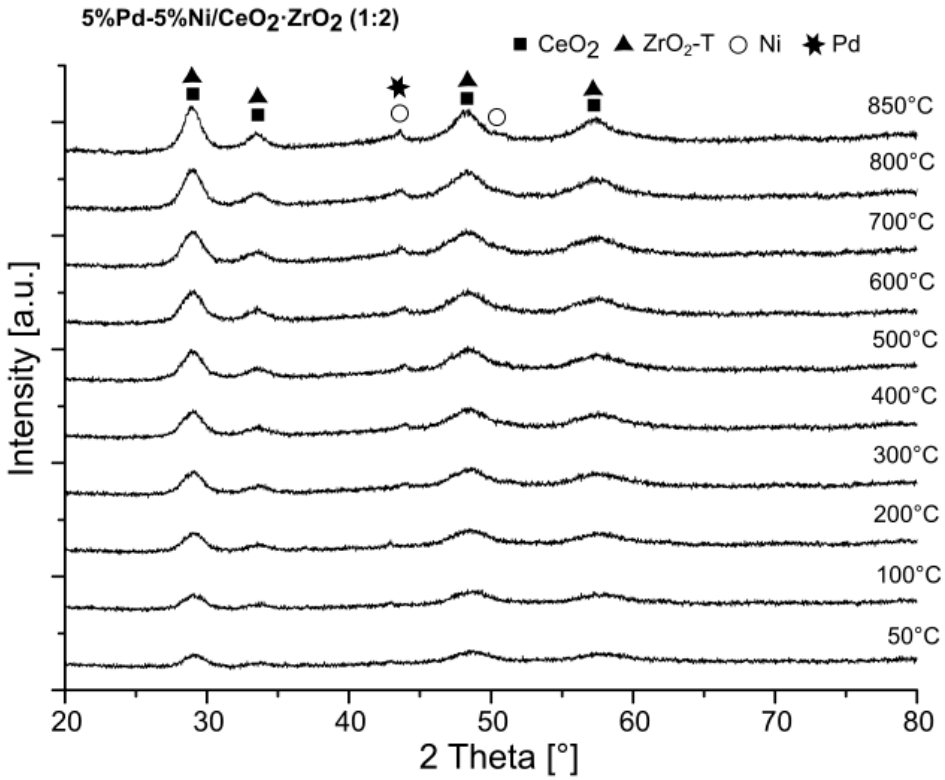

Figure 4. The X-ray diffraction measurements recorded for 5%Pd-5%Ni/CeO_2·ZrO_2 (1:2) catalyst performed the in situ reduction process.

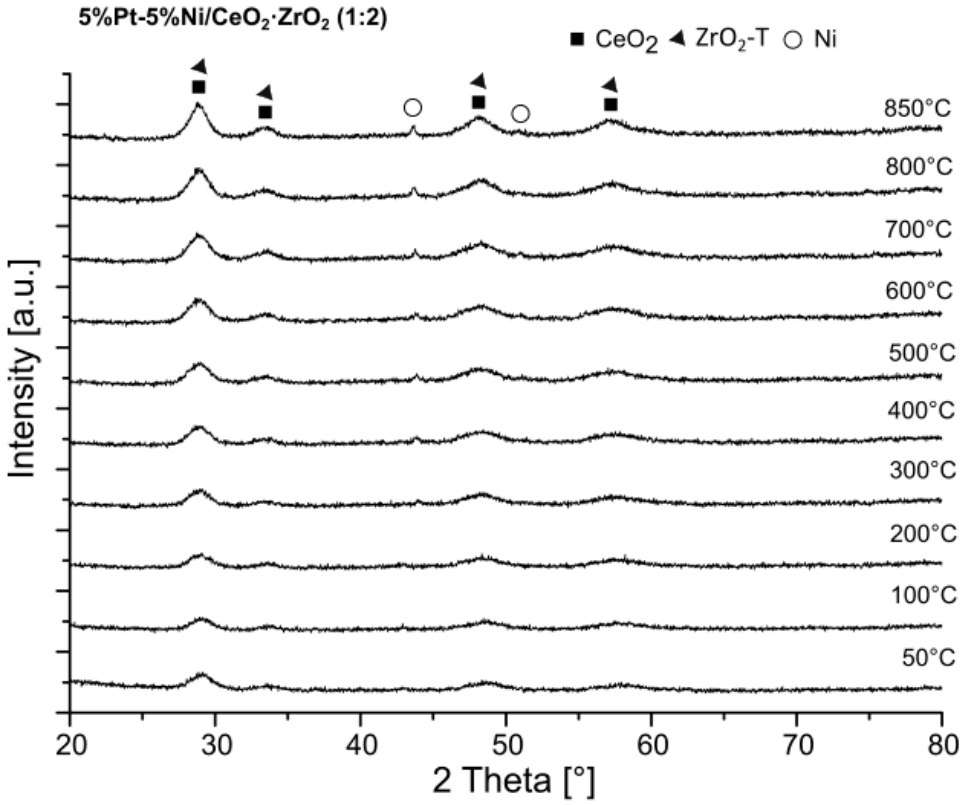

Figure 5. The X-ray diffraction measurements recorded for 5%Pt-5%Ni/CeO_2·ZrO_2 (1:2) catalyst performed the "in situ" reduction process.

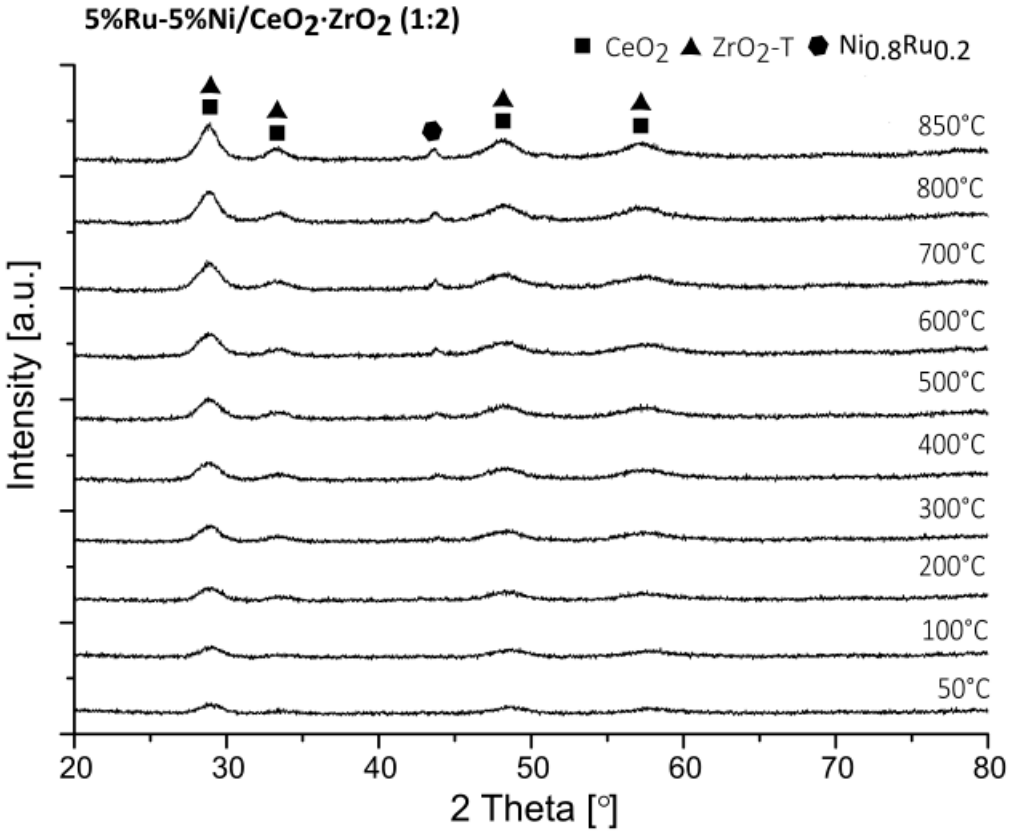

Figure 6. The X-ray diffraction measurements recorded for 5%Ru-5%Ni/CeO_2·ZrO_2 (1:2) catalyst performed the "in situ" reduction process.

In the case of 5%Ag-5%Ni/CeO_2·ZrO_2 (1:2) system (see Figure 3), the nickel oxide reduction occurred at about 300 °C and the metallic Ag appeared in the XRD curve at about 700 °C. The diffraction curve recorded for 5%Ag-5%Ni/CeO_2·ZrO_2 system at 300 °C showed diffraction peaks assigned to CeO_2, ZrO_2, metallic Ni and Ag phases. Rising the reduction temperature up to 850 °C resulted in shifting of the presented reflexes assigned to Ni phase towards the lower 2 theta angles. It is an essential fact that both Ni and Ag crystallize in identical crystallographic systems (regular) and space groups (Fm-3m), which facilitates the formation of solid solutions of these metals [10]. It should be also noted that the main peak (111) of metallic Ag positioned at 2 theta = 37.7 is present in the XRD curve even at 850 °C. It is difficult to unequivocally confirm the alloying in this case due to the presence of the metallic Ni and Ag phases practically at the same values of 2 theta angles, which makes the phase analysis of this system difficult. The observed shift of the described reflexes at high temperature may be associated with the shrinking of the sample or by the alloying process of both metals [10].

The XRD patterns of 5% Pd-5% Ni/CeO_2·ZrO_2 supported catalysts obtained during the reduction process performed in the temperature range 50–850 are given in Figure 4. In this case, also starting from 300 °C the diffraction peaks related to CeO_2, ZrO_2, metallic Ni, and Pd phases were visible in the XRD patterns. The positions of the diffraction peaks attributed to the metallic Ni and Pd are very similar and the unequivocal distinction of these phases in the same sample is very difficult. In addition, it should be emphasized that the lack of reflexes of the metallic Pd phase may also prove the Pd-Ni alloy formation for this catalytic system at high temperature as evidenced by the shift in the reduction peaks assigned to the Ni phase towards lower 2 theta values with the increasing of the reducing temperature.

Analogous phase composition studies were also done for the 5%Pt-5%Ni/CeO_2·ZrO_2 (1:2) bimetallic system (see Figure 5). The X-ray diffraction curve recorded for the 5%Pt-

5%Ni/CeO_2·ZrO_2 (1:2) catalyst confirmed the presence of peaks assigned to NiO and CeO_2 phases on the diffractograms recorded for the bimetallic 5%Pt-5%Ni/CeO_2·ZrO_2 (1:2) system to 200 °C. The metallic Ni phase is visible in the XRD pattern recorded for this system at 300°C. Further increasing of the reduction temperature leads to shifting of the reflexes assigned to metallic Ni towards to lower values of 2 theta angles. The lack of reflexes attributed to metallic Pt may also confirmed the occurrence of an alloying process between Pt and Ni at high temperature. The same phase composition studies were also performed for bimetallic 5% Ru-5% Ni/CeO_2·ZrO_2 (1:2) catalysts in the temperature range of 50–850 °C (see Figure 6). XRD analysis of the 5%Ru-5%Ni/CeO_2·ZrO_2 (1:2) system performed during "in situ" reduction process showed the occurrence of diffraction peaks assigned to CeO_2, ZrO_2 nickel oxide phases up to 200 °C. Rising the reduction temperature to 300 °C results in the appearance of metallic Ni in the XRD pattern. Further increasing of the reduction temperature indicates the formation of an alloy phase between Ru and Ni. The occurrence of this phase was confirmed by the detection of an $Ni_{0.8}Ru_{0.2}$ alloy phase on the diffractograms collected for this bimetallic catalyst at high temperature.

2.5. SEM-EDS Measurements

The composition and morphology of the catalyst surface of the prepared monometallic 5%Ni/CeO_2·ZrO_2 (1:2) and bimetallic 1%Pt-5%Ni/CeO_2·ZrO_2 (1:2), 1%Ag-5%Ni/CeO_2·ZrO_2 (1:2), 1%Pd-5%Ni/CeO_2·ZrO_2 (1:2), 1%Ru-5%Ni/CeO_2·ZrO_2 (1:2) catalysts were determined using a scanning electron microscope equipped with an EDS detector. The SEM-EDS images of the investigated catalysts are presented in Figure 7, clearly confirming their composition. The SEM images collected for the 5%Ni/CeO_2·ZrO_2 (1:2) system showed the presence of the following elements such as Ni, Ce, Zr and O. In the case of bimetallic catalysts, the involved noble metals (Ag, Pt, Pd, and Ru) were also visible on the catalytic surface. It is also worth noting that in the case of Pt-Ni and Ru-Ni bimetallic catalysts, the most homogeneous distribution of noble metals on the surface of catalytic systems was observed. In addition, for these systems, the most homogeneous distribution of nickel on the catalytic systems surface was detected compared to the rest of the investigated catalytic systems. Further SEM-EDS studies were carried out to confirm the existence of interactions between the active phase components. The SEM images and EDS spectra collected for the marked point as well as line analysis were performed and the results are given in Figure 8. The SEM images and EDS spectra recorded for all bimetallic catalysts clearly confirmed that in all marked points Ni and appreciated noble metal elements were detected on the surface of the investigated catalytic systems (see Figure 9). In addition, for the scanned line marked in the images presented in Figure 8 recorded for 1%Pt-5% Ni/CeO_2·ZrO_2 (1:2), 1%Pd-5%Ni/CeO_2·ZrO_2 (1:2), and 1%Ru-5%Ni/CeO_2·ZrO_2 (1:2) bimetallic catalysts, the collected signals assigned to Ni and noble metals indicate that the increasing of Ni elements results in an increase in the corresponding precious metal signal. In the case of the bimetallic 1%Ag-5%Ni/CeO_2·ZrO_2 (1:2) catalyst system, the analysis of the scanned line showed Ag and Ni elements and the surface points with the occurrence of only one element (Ni) in the studied marked area (see Figure 8). This result confirmed the existence specific interactions between metallic nickel and precious metals for all bimetallic catalysts. These results also agree well with the TPR-H_2 and XRD data obtained for 1%Ru-5%Ni/CeO_2·ZrO_2 (1:2) catalyst. In addition, the formation of an alloy in the case of bimetallic 1%Pt-5%Ni/CeO_2·ZrO_2 (1:2) and 1%Pd-5%Ni/CeO_2·ZrO_2 (1:2) cannot be ruled out and can explain the shift of the reflections assigned to the metallic Ni during the reduction of the bimetallic catalysts at high temperature range.

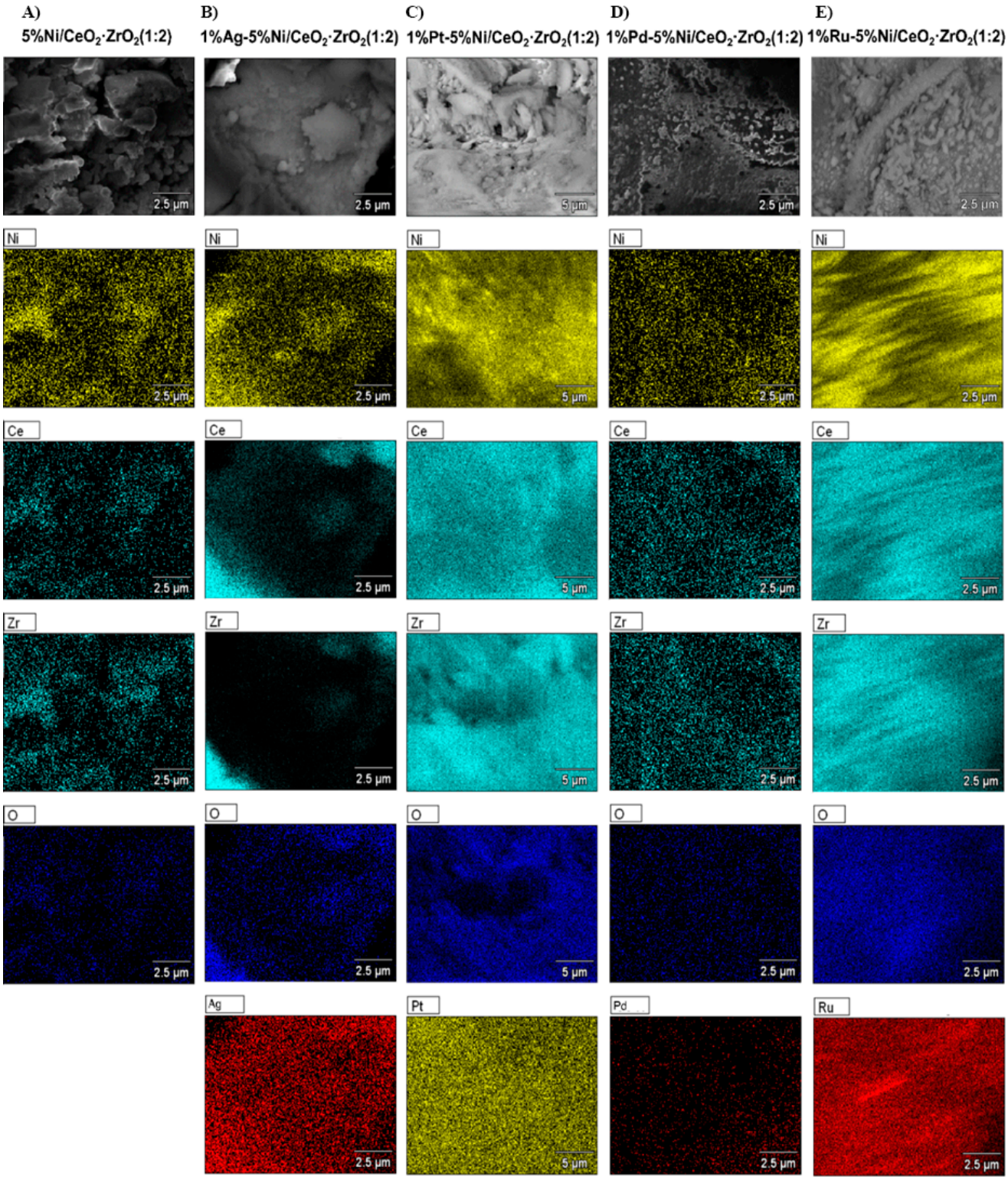

Figure 7. SEM-EDS images of (**A**) monometallic 5%Ni/CeO_2·ZrO_2 (1:2) and bimetallic catalysts (**B**) 1%Ag-5%Ni/CeO_2·ZrO_2 (**C**) 1%Pt-5%Ni/CeO_2·ZrO_2 (**D**) 1%Pd-5%Ni/CeO_2·ZrO_2 (**E**) 1%Ru-5%Ni/CeO_2·ZrO_2 calcined in an air atmosphere at 400 °C for 4 h.

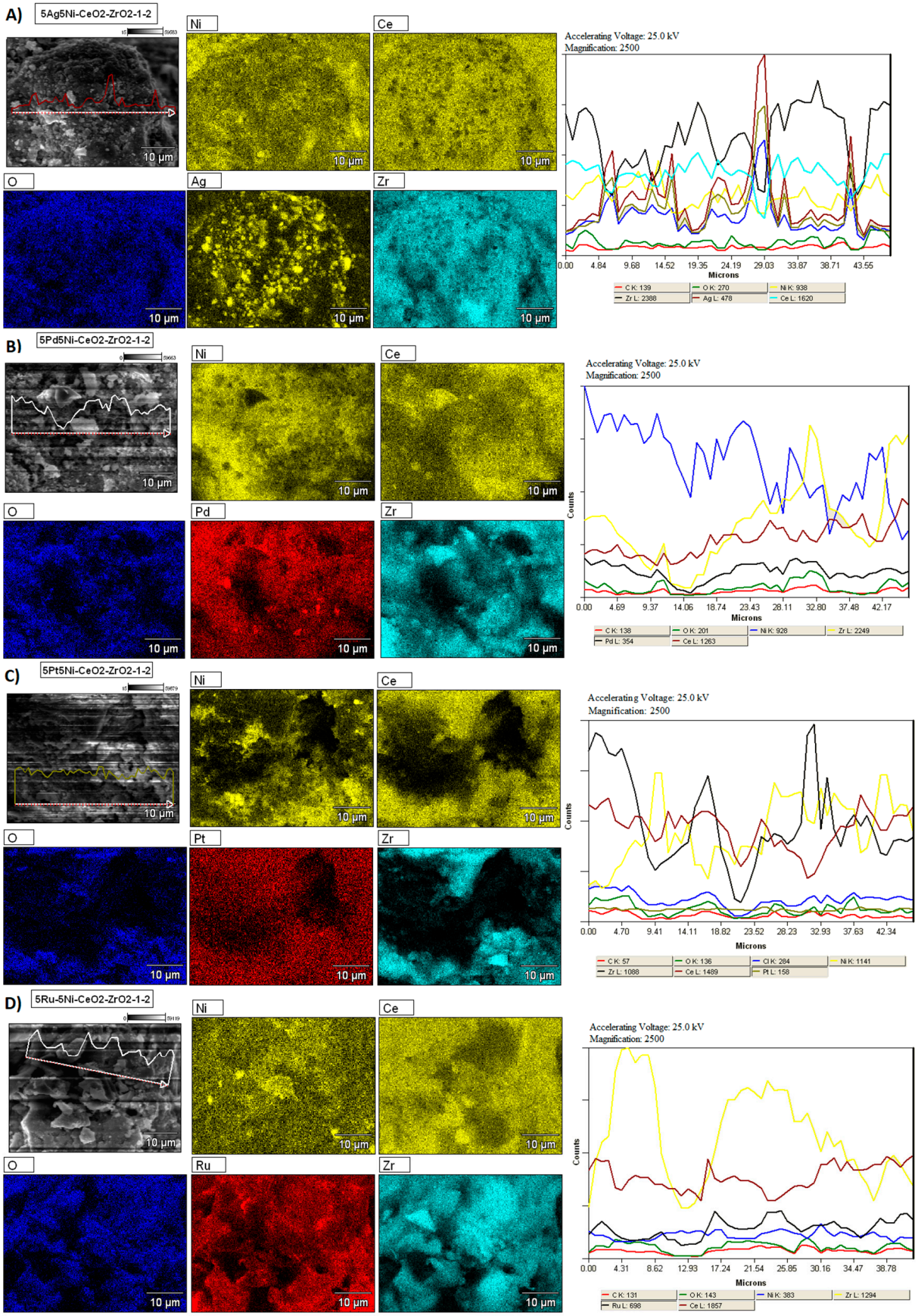

Figure 8. (**A**) SEM image and EDS spectra collected from the marked line analysis recorded for reduced bimetallic 5%Ag-5%Ni/CeO_2·ZrO_2 (1:2) catalyst performed in a mixture of 5%H_2-95%Ar at 500 °C for 1 h; (**B**) SEM image and EDS

spectra collected from the marked line analysis recorded for reduced bimetallic 5%Pd-5%Ni/CeO_2·ZrO_2 (1:2) catalyst performed in a mixture of 5%H_2-95%Ar at 500 °C for 1 h; (**C**) SEM image and EDS spectra collected from the marked line analysis recorded for reduced bimetallic 5%Pt-5%Ni/CeO_2.ZrO_2 (1:2) catalyst performed in a mixture of 5%H_2-95%Ar at 500 °C for 1 h; (**D**) SEM image and EDS spectra collected from the marked line analysis recorded for reduced bimetallic 5%Ru-5%Ni/CeO_2·ZrO_2 (1:2) catalyst performed in a mixture of 5%H_2-95%Ar at 500 °C for 1 h.

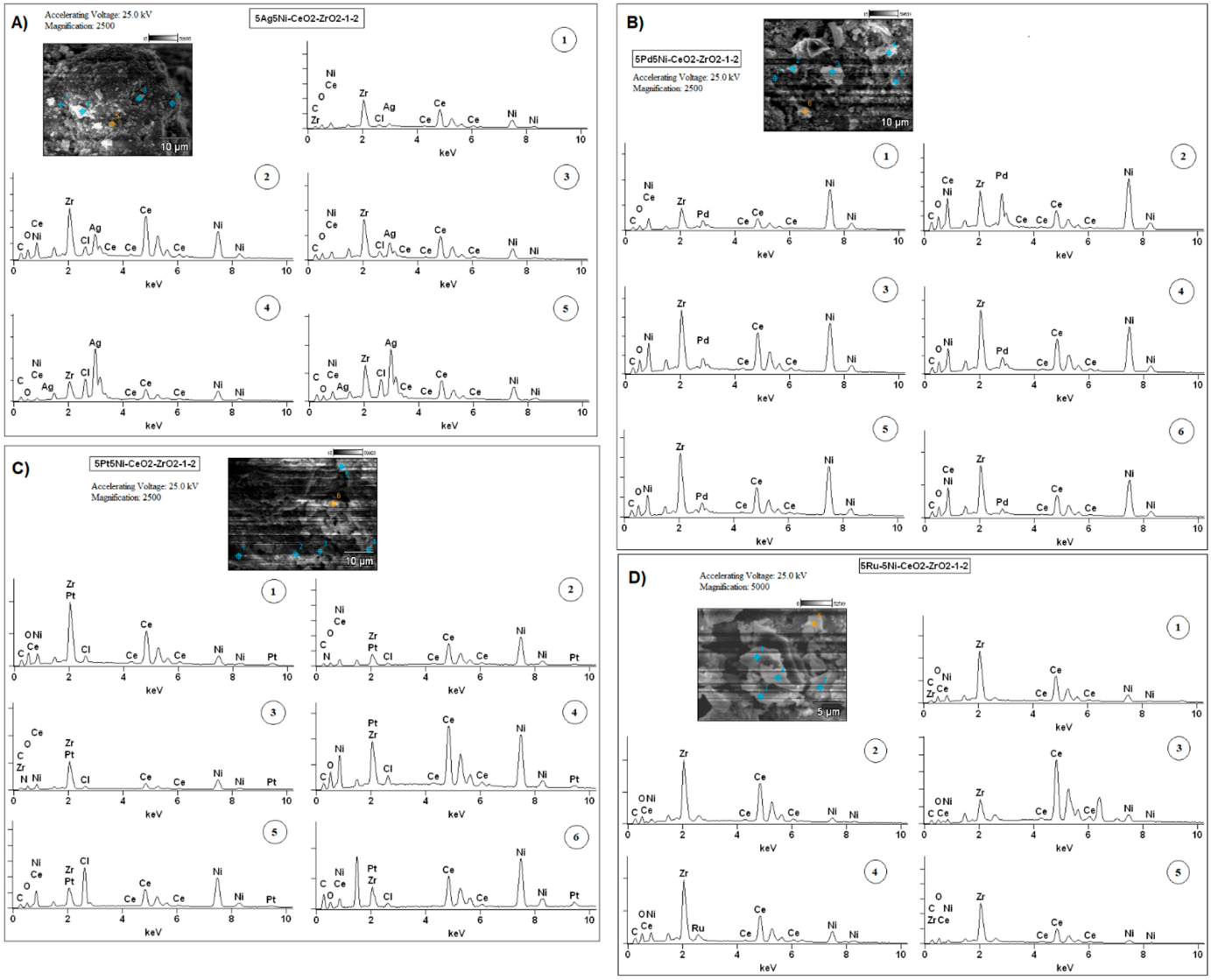

Figure 9. (**A**) SEM image and EDS spectra collected from the marked points analysis recorded for reduced bimetallic 5%Ag-5%Ni/CeO_2·ZrO_2 (1:2) catalyst; (**B**) SEM image and EDS spectra collected from the marked points analysis recorded for reduced bimetallic 5%Pd-5%Ni/CeO2·ZrO_2 (1:2) catalyst; (**C**) SEM image and EDS spectra collected from the marked points analysis recorded for reduced bimetallic 5%Pt-5%Ni/CeO_2·ZrO_2 (1:2) catalyst; (**D**) SEM image and EDS spectra collected from the marked points analysis recorded for reduced bimetallic 5%Ru-5%Ni/CeO_2·ZrO_2 (1:2) catalyst.

2.6. XPS Surface Analysis of the Mono- and Bimetallic Ni Catalysts Supported on CeO_2·ZrO_2 (1:2) System

The interactions between the active phase components were also investigated in this work using XPS technique. The XPS measurements were performed for both calcined and reduced bimetallic catalysts supported on CeO_2·ZrO_2 (1:2). The results of the high-resolution Ni $2p_{3/2}$ XPS spectra and of the precious metals used were done for calcined and reduced monometallic Ni and bimetallic catalysts and are displayed in Figure 10. The Ni $2p_{3/2}$ core-level spectra of 846–896 eV recorded for all bimetallic catalysts for calcined

and reduced systems are given in Figure 10A,B, respectively. The XPS spectra recorded for monometallic Ni and bimetallic catalysts after calcination in an air atmosphere at 400 °C are presented in Figure 10A. The spectra show the characteristic band positioned at 855.6 eV [34] and in the binding energy region 853.7–853.9 which is assigned to Ni^{3+} and NiO species, respectively, present on the catalyst surface. It is also worth emphasizing that in the case of monometallic Ni and bimetallic 5%Ag-5%Ni/CeO_2·ZrO_2 (1:2) catalysts, more intense bands located in the binding energy range 853.7–853.9 can be detected. This behaviour may indicate that the stronger interaction of Ni^{2+} species with support components. In the same Figure 10B, XPS spectra of the reduced catalysts in a mixture of 5%H_2-95%Ar were presented. It can be easily observed in the XPS spectra collected for mono- and bimetallic Ni system the characteristic bands located at about 855.6, in the binding energy range 853.7–853.9 and 852.9 eV [35] assigned to the Ni^{3+}, NiO and Ni^0 species present on the catalysts surface [9], respectively. It is also worth to note that in the case of the reduced mono- and bimetallic catalysts, the specific bands located in the energy range 852–859 eV visible in the spectra are shifted towards lower binding energy range compared to the same bands observed for the calcined catalysts. This behaviour confirms the reduction state of the investigated mono- and bimetallic samples.

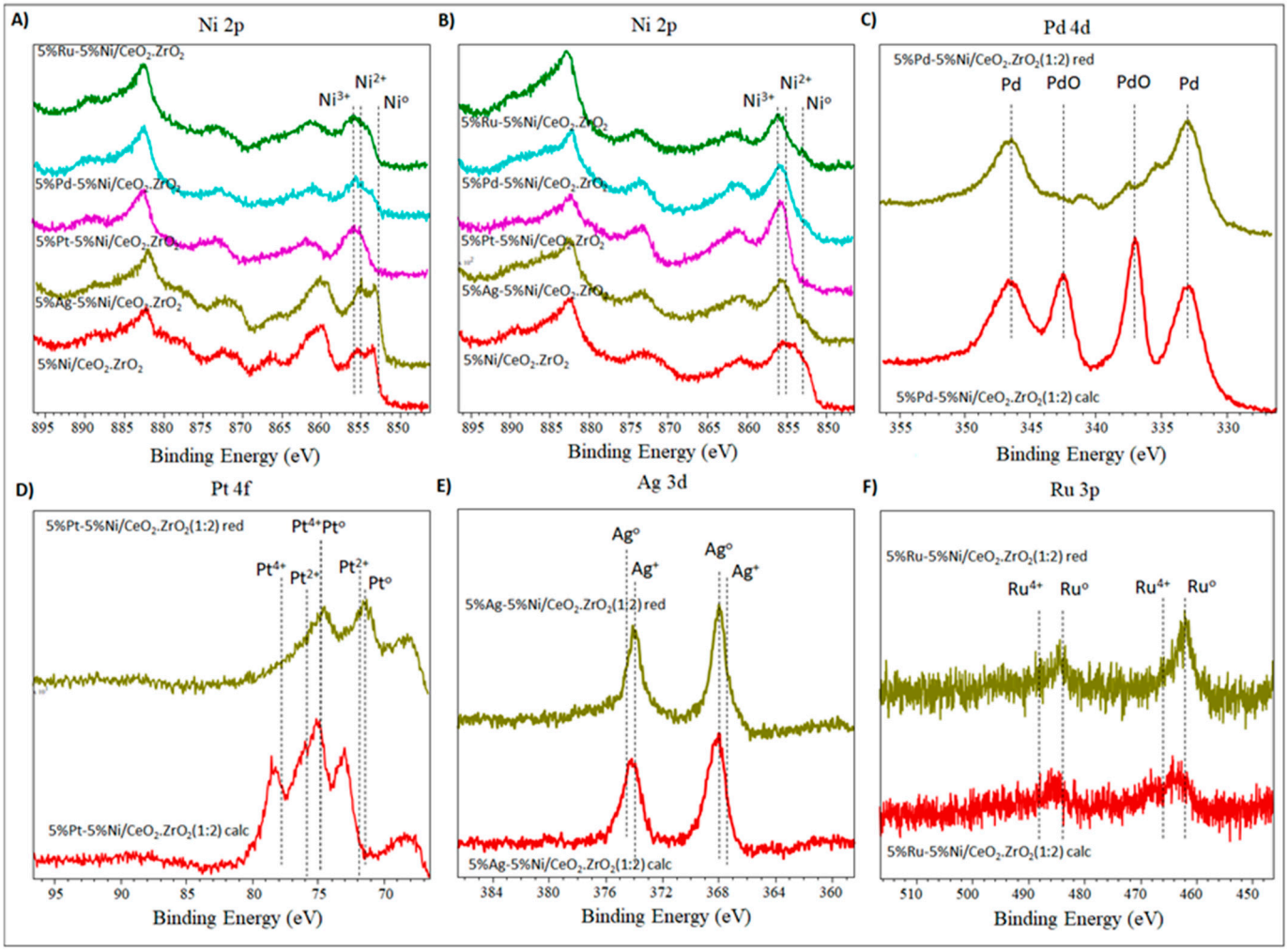

Figure 10. (**A**) Ni 2p XPS of mono- and bimetallic Ni catalysts calcined in an air atmosphere at 400 °C (**B**) Ni 2p XPS of mono- and bimetallic Ni catalysts reduced in a mixture of 5%H_2-95%Ar at 500 °C for 1 h (**C**) Pd 4d XPS of calcined and reduced bimetallic 5%Pd-5%Ni/CeO_2·ZrO_2 (1:2) catalysts (**D**) Pt 4f XPS spectra of calcined and reduced bimetallic 5%Pt-5%Ni/CeO_2·ZrO_2 (1:2) catalysts (**E**) Ag 3d XPS of calcined and reduced bimetallic 5%Ag-5%Ni/CeO_2·ZrO_2 (1:2)catalysts (**F**) Ru 4d XPS of calcined and reduced bimetallic 5%Ru-5%Ni/CeO_2·ZrO_2 (1:2) catalysts.

The Pd 3d spectra of bimetallic 5%Pd-5%Ni/CeO_2·ZrO_2 (1:2) catalysts are shown in Figure 10C. Four main peaks can be easily distinguished in the XPS spectra of the calcined catalysts located at 333, 337, 342.5, and 340.5 eV and 347 eV. The observed peaks are assigned to metallic palladium and PdO [36,37]. The results clearly confirm that the signals assigned to PdO disappear after the reduction process for bimetallic catalysts in a mixture of 5%H_2-95%Ar at 500 °C for 1h. It is also worth to mention that the appearance of low intensity bands assigned to Pd^{2+} species in the case of the reduced samples is due to the oxidation of surface Pd atoms by oxygen from the air. The shifts of the observed bands in the 2p Ni spectra recorded for all bimetallic catalysts in relation to monometallic Ni catalyst may be explained by the alloy formation phase for the catalysts reduced in a mixture of 5%H_2-95%Ar mixture. This behaviour is strongly confirmed by the TPR and XRD measurements performed for all bimetallic catalysts investigated in this work. The authors of the work [38] confirmed an alloy PdNi formation by XPS measurements. They reported that the specific band located in the spectrum of Pd $3d_{5/2}$, the binding energy (BE) was shifted from 335.1 eV to 335.9 eV for the spent catalyst. This observed shift was assigned to the changes of the valence electron density and matrix shift of Pd atoms which was the result of the diffusion of Ni into palladium. Figure 10D presents the XPS analysis of the bimetallic 5%Pt-5%Ni/CeO_2·ZrO_2 (1:2) catalysts also being obtained after calcination and reduction at the same conditions. The bands at 71.4 eV and 75 eV are assigned to metallic Pt, while the Pt^{2+} can be distinguished at about 72.2 and 75.8 eV [39]. While the Pt^{4+} species can be observed at about 72 eV and overlapped with metallic Pt at 74.8 eV. The XPS results obtained for calcined and reduced samples clearly indicate that after reduction, the oxide species practically disappear and due to reduction to metallic platinum [40]. This result may also suggest that a PtNi alloy phase is created, as suggested by the TPR-H_2 and XRD measurements. Figure 10E shows the maxima of the characteristic XPS bands located at about 374 eV and 368 for the Ag containing catalyst after calcination. However, in the case of the reduced sample (5%Ag-5%Ni/CeO_2·ZrO_2 (1:2)), the characteristic bands are shifted towards lower binding energies compared to the calcined catalyst. This result may be explained by the specific interaction between metallic Ag and Ni species, which is manifested by the reduction studies presented in this work (see the reduction studies of bimetallic 5%Ag-5%Ni/CeO_2·ZrO_2 (1:2) catalysts). Normally, the XPS bands assigned to metallic Ag are positioned at 368.2 eV ($Ag3d_{5/2}$) and at 374.2 eV ($Ag3d_{3/2}$), while the Ag_2O species are identified at 367.8 eV ($Ag3d_{5/2}$) and at 374.0 eV ($3d_{3/2}$), respectively [41,42]. The shifts of the specific XPS bands assigned to metallic Ag towards lower binding energy indicate of a specific interaction between silver and support or active phase component (metallic Ni). Such a result may also indicate the alloy formation between silver with nickel. Other authors [43] also reported that they observed in the Ag 3d spectrum the Ag $3d_{5/2}$ and Ag $3d_{3/2}$ peaks occurring at the binding energies of 368.2 and 374.2 eV, respectively, with a difference of 6.0 eV which were assigned to metallic Ag in a AgNi alloy. Figure 10F presents the XPS spectra for bimetallic 5%Ru-5%Ni/CeO_2·ZrO_2 (1:2) calcined and reduced catalysts. One can distinguish the peaks positioned at 462.2 eV and 484.4 eV assigned to metallic Ru and also two XPS bands located at the binding energy at 466.1 eV and 488.6 eV attributed to Ru^{4+} species. The comparison of the two XPS spectra for calcined and reduced catalysts shows that the Ru^{4+} peaks disappears after the reduction process. The same value of the specific bands located at 462.2 eV and 484.4 eV were assigned to metallic Ru were detected by other authors who assigned the XPS signals to the 5%Ru-5%Ni/CeO_2·ZrO_2 (1:2) alloy phase [44].

3. Materials and Methods

3.1. Catalytic Material Preparation

The binary oxide support (CeO_2·ZrO_2 (1:2)) was synthesized by a co-precipitation method. Appropriate amounts of cerium nitrate and zirconium nitrate were mixed and ammonia solution was used as a precipitation agent. The obtained precipitate was washed, filtered, and dried at 120 °C for 12 h. Then, the support was calcined in an air stream at

400 °C for 4 h. In the next step, a monometallic nickel supported catalyst was prepared using a wet impregnation method and nickel nitrate solution was used as a metal precursor. The impregnation process lasted 12 h and after then the solution was evaporated and dried at 80 °C for 2 h and calcined in an air at 400 °C for 4 h. The nickel concentration in the monometallic catalyst was 5%. The subsequent impregnation method was used also to prepare bimetallic Ag, Pd, Pt, Ru-Ni catalysts supported on $CeO_2 \cdot ZrO_2$ (1:2) carrier. The noble metal loading in all cases was 1 wt. % of metal. The procedure for preparing bimetallic catalysts contained the same steps and conditions, which were applied for the monometallic Ni catalyst supported on a binary oxide support.

3.2. Characterization Techniques

The reducibility of the synthesized catalytic systems was investigated using Temperature programmed reduction (TPR-H_2) technique carried out in an automatic AMI-1 apparatus (Altamira Instruments, Pittsburgh, PA, USA). In each measurement, about 0.1 g sample was used and the reduction behaviour was studied in the temperature range 25–900 °C. Temperature programmed desorption of ammonia (TPD-NH_3) analysis was used to determine the acidity of the surface of the investigated catalytic materials. In the case of mono- and bimetallic supported catalysts, before each TPD-NH_3 test, the sample was reduced "in situ" at 500 °C in a mixture of 5%H_2-95%Ar. The TPD-NH_3 experiments were performed in the temperature range 100–600 °C and NH_3 was used as a probe molecule. X-ray diffraction (XRD) studies were carried out on PANalytical X'Peert Pro MPD diffractometer and using K_α radiation of Cu at 1.5405 Å in the 2Θ angle range 5–90° (Malvern Panalytical Ltd., Malvern, UK). The surface morphology was investigated using S-4700 Scanning Electron Microscopy HITACHI (Tokyo, Japan), equipped with an energy dispersive spectrometer (ThermoNoran, Madison, WI, USA) (SEM-EDS). XPS measurements were carried out on a Kratos AXIS Ultra DLD spectrometer (Kratos Analytical Ltd., Manchester, UK) equipped with monochromatic Al source run at 15 keV and 15 mA. Spectra were collected with a pass energy of 160 eV and high-resolution spectra were obtained using a 20 eV pass energy. The processing of spectra was performed using Casa XPS software and all binding energies were referenced to the neutral carbon peak at 285.0 eV.

3.3. Catalytic Activity Tests in Oxy-Steam Reforming of Liquified Natural Gas (OSR-LNG)

The catalytic activity tests of the mono- and bimetallic catalysts supported on binary oxide $CeO_2 \cdot ZrO_2$ (1:2) were carried out in the oxy-steam reforming of liquefied natural gas reaction (OSR-LNG). In each catalytic test, a 0.2 g catalyst sample was placed in a quartz microreactor and the activity was measured after 30 min of stabilization under atmospheric pressure. The catalyst bed has a diameter equal 6 mm and height about 10 mm, respectively. All the activity tests were performed under atmospheric pressure in the temperature range 400–900 °C. The total gas flow rate of the reaction mixture was 51 cm^3/min. The composition of the reaction mixture was constant during the activity test. During all catalytic activity measurements a model gas mixture of LNG (5% CH_4, 0.4% C_2H_6, 0.2% C_3H_8, 0.05% C_4H_{10} and 94.35% Ar) and a mixture of 5% O_2/95% Ar were used. The molar ratio between reagents in the reaction mixture was CH_4:H_2O:O_2 = 1:2.7:0.35, respectively. The gaseous products of the OSR-LNG reaction were analysed using gas chromatograph equipped with TCD and FID detector. The organic products were analysed using an online gas chromatograph equipped with a 80/100 HAYE SEP-Q column (RESTEK, Bellefonte, PA, USA). The H_2, CO and CO_2 products were analysed using online gas chromatograph equipped with a 80/100 silicagel packed column. The activity results were expressed as hydrocarbons (methane, ethane, propane, butane) conversion, selectivities to the CO and CO_2 and hydrogen yield. All these values were calculated based on the following equations:

$$C_XH_{Y\,Conv.} = \left(1 - \frac{n - out_{C_xH_Y}}{n - in_{C_xH_Y}}\right) \times 100\ \%$$

$$CO_{Sel.} = \left(\frac{n - out_{CO}}{n - out_{CO} + n - out_{CO2}} \right) \times 100\ \%$$

$$CO_{2Sel.} = \left(\frac{n - out_{CO2}}{n - out_{CO} + n - out_{CO2}} \right) \times 100\ \%$$

$$H_{2Yield} = \left(\frac{\frac{n - out_{H_2}}{2.73}}{\sum(n - in_{C_xH_Y}) - \sum(n - out_{C_xH_Y})} \right) \times 100\ \%$$

where:

$n - in_{C_xH_Y}$—the moles of hydrocarbon (methane, ethane, propane, and butane) at the reactor inlet;
$n - out_{C_xH_Y}$—the moles of hydrocarbon (methane, ethane, propane, and butane) at the reactor outlet;
$n - out_{CO}$—the moles of the CO at the reactor outlet;
$n - out_{CO2}$—the moles of the CO_2 at the reactor outlet;
$n - out_{H_2}$—the moles of the H_2 at the reactor outlet;
$\sum(n - in_{C_xH_Y})$—the sum of the moles of the hydrocarbons (methane, ethane, propane, and butane) at the reactor inlet;
$\sum(n - out_{C_xH_Y})$—the sum of the moles of the hydrocarbons (methane, ethane, propane, and butane) at the reactor outlet.

4. Conclusions

Novel bimetallic Pd-Ni, Pt-Ni, Ag-Ni or Ru-Ni catalysts supported on $CeO_2{\cdot}ZrO_2$ (1:2) binary oxide support were prepared via an impregnation method and tested for the first time in the process of oxygen-steam reforming of LNG for hydrogen production. The catalysts' physicochemical properties were studied using a spectrum of techniques including TPR-H_2, TPD-NH_3, XPS, conventional and in-situ XRD methods and SEM-EDS and correlated with the reactivity results. The activity tests showed that the most promising among all bimetallic materials were the 1%Ru-5%Ni/$CeO_2{\cdot}ZrO_2$ (1:2) and 1%Pt-5%Ni/$CeO_2{\cdot}ZrO_2$ (1:2) systems which exhibited the highest light hydrocarbon conversion at 600 °C with the highest yield of hydrogen formation. This result can be explained by the formation of an alloy between Ni and the noble metal (Pt, Ru). In addition, the bimetallic 1%Pt-5%Ni/$CeO_2{\cdot}ZrO_2$ (1:2) and 1%Ru-5%Ni/$CeO_2{\cdot}ZrO_2$ (1:2) catalysts showed the lowest strong acid centers on the catalyst surface and the highest content of NiO species that weakly interacted with support compared to the rest of the investigated catalyst systems. The occurrence of an alloy $Ru_{0.2}$-$Ni_{0.8}$ phase in the case of the investigated 5%Ru-5%Ni/$CeO_2{\cdot}ZrO_2$ (1:2) bimetallic catalysts was detected from the diffraction patterns. The XRD, XPS, TPR and SEM-EDS results also confirmed that the alloy formation between Pt and Ni and between Pd and Ni for the investigated bimetallic catalysts cannot be ruled out. In addition, based on the XPS and XRD results obtained for bimetallic 5%Ag-5%Ni/$CeO_2{\cdot}ZrO_2$ (1:2) catalysts, the formation of an alloy between nickel and silver cannot be also ruled out. The obtained reactivity results obtained in the oxy-steam reforming of LNG process clearly confirmed the potential application of bimetallic 1%Pt-5%Ni/$CeO_2{\cdot}ZrO_2$ (1:2) and 1%Ru-5%Ni/$CeO_2{\cdot}ZrO_2$ (1:2) systems as an active material for hydrogen production in fuel cell technology.

Author Contributions: The work was designed and presented by M.M., K.V., M.I.S.-J., W.M. and P.M. All authors have read and agreed to the published version of the manuscript.

Funding: The authors gratefully acknowledge that this work was financially supported by the National Science Centre (NCN) in Poland within the "OPUS" Programme (Grant no. 2018/29/B/ST8/01317).

Data Availability Statement: The results presented in this work were not previously published anywhere.

Conflicts of Interest: The authors declare no conflict of interest.

References

1. Mierczynski, P.; Mierczynska, A.; Maniukiewicz, W.; Maniecki, T.P.; Vasilev, K. MWCNTs as a catalyst in oxy-steam reforming of methanol. *RSC Adv.* **2016**, *6*, 81408–81413. [CrossRef]
2. Gupta, R.B. *Hydrogen Fuel: Production, Transport, and Storage*; CRC Press: Boca Raton, FL, USA, 2008.
3. Ji, M.; Wang, J. Review and comparison of various hydrogenproduction methods based on costs and life cycleimpact assessment indicators. *Int. J. Hydrogen Energy* **2021**, *46*, 38612–38635. [CrossRef]
4. Mierczynski, P.; Mosinska, M.; Maniukiewicz, W.; Nowosielska, M.; Czylkowska, A.; Szynkowska, M.I. Oxy-steam reforming of methanol on copper catalysts. *React. Kinet. Mech. Catal.* **2019**, *127*, 857–874. [CrossRef]
5. Mierczynski, P.; Mosinska, M.; Maniukiewicz, W.; Vasilev, K.; Szynkowska, M.I. Novel Rh(Pd)-Cu(Ni) supported catalysts for oxy-steam reforming of methanol. *Arab. J. Chem.* **2018**, *13*, 3183–3195. [CrossRef]
6. Mierczynski, P.; Mosinska, M.; Zakrzewski, M.; Dawid, B.; Ciesielski, R.; Maniecki, T.; Maniukiewicz, W. Influence of the Zn–Al binary oxide composition on the physicochemical and catalytic properties of Ni catalysts in the oxy-steam reforming of methanol. *React. Kinet. Mech. Catal.* **2017**, *121*, 453–472. [CrossRef]
7. Mierczynski, P.; Mierczynska, A.; Ciesielski, R.; Mosinska, M.; Nowosielska, M.; Czylkowska, A.; Maniukiewicz, W.; Szynkowska, M.I.; Vasilev, K. High Active and Selective Ni/CeO_2–Al_2O_3 and Pd–Ni/CeO_2–Al_2O_3 Catalysts for Oxy-Steam Reforming of Methanol. *Catalysts* **2018**, *8*, 380. [CrossRef]
8. Gil Seo, J.; Youn, M.H.; Park, S.; Lee, J.; Lee, S.H.; Lee, H.; Song, I.K. Hydrogen production by steam reforming of LNG over Ni/Al_2O_3-ZrO_2 catalysts: Effect of ZrO_2 and preparation method of Al_2O_3-ZrO_2. *Korean J. Chem. Eng.* **2008**, *25*, 95–98. [CrossRef]
9. Mierczynski, P.; Mosinska, M.; Stepinska, N.; Chalupka, K.; Nowosielska, M.; Maniukiewicz, W.; Rogowski, J.; Goswami, N.; Vasilev, K.; Szynkowska, M.I. Effect of the support composition on catalytic and physicochemical properties of Ni catalysts in oxy-steam reforming of methane. *Catal. Today* **2020**, *364*, 46–60. [CrossRef]
10. Mosinska, M.; Stepinska, N.; Chalupka, K.; Maniukiewicz, W.; Szynkowska, M.I.; Mierczynski, P. Effect of Ag-Addition on the Catalytic and Physicochemical Properties of Ni/ZrO_2 Catalyst in Oxy-Steam Reforming of CH_4 and LNG Processes. *Catalysts* **2020**, *10*, 855. [CrossRef]
11. Mosinska, M.; Szynkowska, M.I.; Mierczynski, P. Oxy-Steam Reforming of Natural Gas on Ni Catalysts—A Minireview. *Catalysts* **2020**, *10*, 896. [CrossRef]
12. Park, S.; Yoo, J.; Han, S.J.; Song, J.H.; Lee, E.J.; Song, I.K. Steam reforming of liquefied natural gas (LNG) for hydrogen production over nickel–boron–alumina xerogel catalyst. *Int. J. Hydrogen Energy* **2017**, *42*, 15096–15106. [CrossRef]
13. Gil Seo, J.; Youn, M.H.; Park, S.; Chung, J.S.; Song, I.K. Hydrogen production by steam reforming of liquefied natural gas (LNG) over Ni/Al_2O_3–ZrO_2 xerogel catalysts: Effect of calcination temperature of Al_2O_3–ZrO_2 xerogel supports. *Int. J. Hydrogen Energy* **2009**, *34*, 3755–3763. [CrossRef]
14. Bang, Y.; Park, S.; Han, S.J.; Yoo, J.; Song, J.H.; Choi, J.H.; Kang, K.H.; Song, I.K. Hydrogen production by steam reforming of liquefied natural gas (LNG) over mesoporous Ni/Al_2O_3 catalyst prepared by an EDTA-assisted impregnation method. *Appl. Catal. B Environ.* **2015**, *180*, 179–188. [CrossRef]
15. Bang, Y.; Han, S.J.; Yoo, J.; Choi, J.H.; Lee, J.K.; Song, J.H.; Lee, J.; Song, I.K. Hydrogen production by steam reforming of simulated liquefied natural gas (LNG) over nickel catalyst supported on mesoporous phosphorus-modified alumina xerogel. *Appl. Catal. B Environ.* **2013**, *148–149*, 269–280. [CrossRef]
16. Bang, Y.; Gil Seo, J.; Song, I.K. Hydrogen production by steam reforming of liquefied natural gas (LNG) over mesoporous Ni–La–Al_2O_3 aerogel catalysts: Effect of La content. *Int. J. Hydrogen Energy* **2011**, *36*, 8307–8315. [CrossRef]
17. Gil Seo, J.; Youn, M.H.; Song, I.K. Hydrogen production by steam reforming of LNG over Ni/Al_2O_3–ZrO_2 catalysts: Effect of Al_2O_3–ZrO_2 supports prepared by a grafting method. *J. Mol. Catal. A Chem.* **2007**, *268*, 9–14. [CrossRef]
18. Bang, Y.; Han, S.J.; Gil Seo, J.; Youn, M.H.; Song, J.H.; Song, I.K. Hydrogen production by steam reforming of liquefied natural gas (LNG) over ordered mesoporous nickel–alumina catalyst. *Int. J. Hydrogen Energy* **2012**, *37*, 17967–17977. [CrossRef]
19. Armor, J. The multiple roles for catalysis in the production of H_2. *Appl. Catal. A Gen.* **1999**, *176*, 159–176. [CrossRef]
20. Matsumura, Y.; Nakamori, T. Steam reforming of methane over nickel catalysts at low reaction temperature. *Appl. Catal. A Gen.* **2004**, *258*, 107–114. [CrossRef]
21. Dantas, S.C.; Escritori, J.C.; Soares, R.R.; Hori, C.E. Effect of different promoters on Ni/$CeZrO_2$ catalyst for autothermal reforming and partial oxidation of methane. *Chem. Eng. J.* **2010**, *156*, 380–387. [CrossRef]
22. Wu, H.; Pantaleo, G.; La Parola, V.; Venezia, A.M.; Collard, X.; Aprile, C.; Liotta, L.F. Bi- and trimetallic Ni catalysts over Al_2O_3 and Al_2O_3-MO (M = Ce or Mg) oxides for methane dry reforming: Au and Pt additive effects. *Appl. Catal. B Environ.* **2014**, *156–157*, 350–361. [CrossRef]
23. Takeguchi, T.; Furukawa, S.-N.; Inoue, M.; Eguchi, K. Autothermal reforming of methane over Ni catalysts supported over CaO–CeO_2–ZrO_2 solid solution. *Appl. Catal. A Gen.* **2003**, *240*, 223–233. [CrossRef]
24. Mierczynski, P. Comparative Studies of Bimetallic Ru–Cu, Rh–Cu, Ag–Cu, Ir–Cu Catalysts Supported on ZnO–Al_2O_3, ZrO_2–Al_2O_3 Systems. *Catal. Lett.* **2016**, *146*, 1825–1837. [CrossRef]
25. Mierczynski, P.; Vasilev, K.; Mierczynska, A.; Maniukiewicz, W.; Maniecki, T. Highly selective Pd–Cu/$ZnAl_2O_4$ catalyst for hydrogen production. *Appl. Catal. A Gen.* **2014**, *479*, 26–34. [CrossRef]
26. Ashok, J.; Ang, M.; Kawi, S. Enhanced activity of CO_2 methanation over Ni/CeO_2-ZrO_2 catalysts: Influence of preparation methods. *Catal. Today* **2016**, *281*, 304–311. [CrossRef]

27. Mierczynski, P.; Ciesielski, R.; Kedziora, A.; Shtyka, O.; Maniecki, T. Methanol Synthesis Using Copper Catalysts Supported on $CeO_2-Al_2O_3$ Mixed Oxide. *Fibre Chem.* **2016**, *48*, 271–275. [CrossRef]
28. Zheng, Y.; Li, K.; Wang, H.; Wang, Y.; Tian, D.; Wei, Y.; Zhu, X.; Zeng, C.; Luo, Y. Structure dependence and reaction mechanism of CO oxidation: A model study on macroporous CeO_2 and CeO_2-ZrO_2 catalysts. *J. Catal.* **2016**, *344*, 365–377. [CrossRef]
29. Pérez-Hernández, R.; Gutiérrez-Martínez, A.; Palacios, J.; Vega-Hernández, M.; Rodríguez-Lugo, V. Hydrogen production by oxidative steam reforming of methanol over Ni/CeO_2–ZrO_2 catalysts. *Int. J. Hydrogen Energy* **2011**, *36*, 6601–6608. [CrossRef]
30. Xie, J.; Sun, X.; Barrett, L.; Walker, B.R.; Karote, D.R.; Langemeier, J.M.; Leaym, X.; Kroh, F.; Traylor, W.; Feng, J.; et al. Autothermal reforming and partial oxidation of n-hexadecane via Pt/Ni bimetallic catalysts on ceria-based supports. *Int. J. Hydrogen Energy* **2015**, *40*, 8510–8521. [CrossRef]
31. Mierczynski, P.; Ciesielski, R.; Kedziora, A.; Zaborowski, M.; Maniukiewicz, W.; Nowosielska, M.; Szynkowska, M.I.; Maniecki, T.P. Novel Pd-Cu/$ZnAl_2O_4$-ZrO_2 Catalysts for Methanol Synthesis. *Catal. Lett.* **2014**, *144*, 723–735. [CrossRef]
32. Mierczynski, P.; Maniukiewicz, W.; Maniecki, T.P. Comparative studies of Pd, Ru, Ni, Cu/ZnAl2O4 catalysts for the water gas shift reaction. *Open Chem.* **2013**, *11*, 912–919. [CrossRef]
33. Mierczynski, P.; Stępińska, N.; Mosinska, M.; Chalupka, K.; Albinska, J.; Maniukiewicz, W.; Rogowski, J.; Nowosielska, M.; Szynkowska, M.I. Hydrogen Production via the Oxy-Steam Reforming of LNG or Methane on Ni Catalysts. *Catalysts* **2020**, *10*, 346. [CrossRef]
34. Mierczynski, P.; Vasilev, K.; Mierczynska, A.; Maniukiewicz, W.; Szynkowska, M.I.; Maniecki, T.P. Bimetallic Au–Cu, Au–Ni catalysts supported on MWCNTs for oxy-steam reforming of methanol. *Appl. Catal. B Environ.* **2016**, *185*, 281–294. [CrossRef]
35. Chen, Y.S.; Kang, J.F.; Chen, B.; Gao, B.; Liu, L.F.; Liu, X.Y.; Wang, Y.Y.; Wu, L.; Yu, H.Y.; Wang, J.Y.; et al. Microscopic mechanism for unipolar resistive switching behaviour of nickel oxides. *J. Phys. D Appl. Phys.* **2012**, *45*, 65303. [CrossRef]
36. Jin, Q.; He, Y.; Miao, M.; Guan, C.; Du, Y.; Feng, J.; Li, D. Highly selective and stable PdNi catalyst derived from layered double hydroxides for partial hydrogenation of acetylene. *Appl. Catal. A Gen.* **2015**, *500*, 3–11. [CrossRef]
37. Reddy, G.K.; Ling, C.; Peck, T.C.; Jia, H. Understanding the chemical state of palladium during the direct NO decomposition—Influence of pretreatment environment and reaction temperature. *RSC Adv.* **2017**, *7*, 19645–19655. [CrossRef]
38. Zhang, Q.; Li, Y.; Chai, R.; Zhao, G.; Liu, Y.; Lu, Y. Low-temperature active, oscillation-free PdNi(alloy)/Ni-foam catalyst with enhanced heat transfer for coalbed methane deoxygenation via catalytic combustion. *Appl. Catal. B Environ.* **2016**, *187*, 238–248. [CrossRef]
39. Khalakhan, I.; Vega, L.; Vorokhta, M.; Skála, T.; Viñes, F.; Yakovlev, Y.; Neyman, K.M.; Matolínová, I. Irreversible structural dynamics on the surface of bimetallic PtNi alloy catalyst under alternating oxidizing and reducing environments. *Appl. Catal. B Environ.* **2019**, *264*, 118476. [CrossRef]
40. Mazzotta, E.; Rella, S.; Turco, A.; Malitesta, C. XPS in development of chemical sensors. *RSC Adv.* **2015**, *5*, 83164–83186. [CrossRef]
41. Yurderi, M.; Bulut, A.; Zahmakiran, M.; Kaya, M. Carbon supported trimetallic PdNiAg nanoparticles as highly active, selective and reusable catalyst in the formic acid decomposition. *Appl. Catal. B Environ.* **2014**, *160–161*, 514–524. [CrossRef]
42. Firet, N.J.; Blommaert, M.A.; Burdyny, T.; Venugopal, A.; Bohra, D.; Longo, A.; Smith, W.A. Operando EXAFS study reveals presence of oxygen in oxide-derived silver catalysts for electrochemical CO_2 reduction. *J. Mater. Chem. A* **2019**, *7*, 2597–2607. [CrossRef]
43. Kumar, M.; Deka, S. Multiply Twinned AgNi Alloy Nanoparticles as Highly Active Catalyst for Multiple Reduction and Degradation Reactions. *ACS Appl. Mater. Interfaces* **2014**, *6*, 16071–16081. [CrossRef] [PubMed]
44. Zhu, L.; Sun, H.; Zheng, J.; Yu, C.; Zhang, N.; Shu, Q.; Chen, B.H. Combining Ru, Ni and $Ni(OH)_2$ active sites for improving catalytic performance in benzene hydrogenation. *Mater. Chem. Phys.* **2017**, *192*, 8–16. [CrossRef]